CRAIG O. SAVAGE
BILL MORAN
Raytheon Missile Systems
Guidance, Navigation & Control
1151 E. Hermans Rd.
Tuscon, AZ 85706
E-mail: (c.savage@ee.unimelb.edu.au)

REFERENCES

[1] Kalandros, M., and Pao, L. Y.
Covariance control for multisensor systems.
IEEE Transactions on Aerospace and Electronic Systems, **38**, 4 (Oct. 2000), 1138–1157.

[2] Bar-Shalom, Y., and Xiao-Rong, L.
Estimation and Tracking: Principles, Techniques, and Software.
Norwood, MA: Artech House, 1993.

[3] Bar-Shalom, Y., and Xiao-Rong, L.
Multitarget-Multisensor Tracking: Principles and Techniques (a.k.a. "The Yellow Book").
Storrs, CT: YBS Publishing, 1995

[4] Kershaw, D., and Evans, R.
Adaptive waveform selection for tracking in clutter.
Proceedings of the American Control Conference, Baltimore, MD, June, 1994.

[5] Kershaw, D., and Evans, R.
Optimal waveform selection for tracking systems.
IEEE Transactions on Information Theory, **40**, 5 (Sept. 1994), 1536–1550.

[6] Kershaw, D., and Evans, R.
Waveform selective probabilistic data association.
IEEE Transactions on Aerospace and Electronic Systems, **33** (Oct. 1997), 1180–1188.

[7] La Scala, B., Moran, B., and Evans, R.
Optimal adaptive waveform selection for target detection.
Radar 2003: International Conference on Radar. Adelaide, Australia, Sept. 2003.

[8] Niu, R., Willett, P., and Bar-Shalom, Y.
Tracking considerations in selection of radar waveform for range and range-rate measurements.
IEEE Transactions on Aerospace and Electronic Systems, **38**, 2 (Apr. 2002), 467–487.

[9] Niu, R., Willett, P., and Bar-Shalom, Y.
Further analysis of waveform effects on tracking performance.
Aerospace Conference Proceedings, vol. 3, 2000, 417–431.

[10] Rago, C., Willett, P., and Bar-Shalom, Y.
Detection-tracking performance with combined waveforms.
IEEE Transactions on Aerospace and Electronic Systems, **34**, 2 (1998), 612–624.

[11] Fielding, P. J., and Kinghorn, A. M.
Waveform optimisation for efficient resource allocation in airborne AESA radar systems.
In *Multifunction Radar and Sonar Sensor Management Techniques*. IEE, Nov. 26, 2001.

[12] van Trees, H.
Detection, Estimation, and Modulation Theory, Part III.
New York: Wiley, 1968.

[13] Borden, B.
The fractional Fourier transform and ISAR imaging.
Inverse Problems, **16**, 2 (Apr. 2000), Available online at http://www.iop.org, as of Sept. 1, 2004.

[14] Ozaktas, H. M., and Kutay, M. A.
Effect of fractional Fourier transformation on time-frequency distributions belonging to the Cohen class.
IEEE Transactions on Signal Processing Letters, **40**, 1 (1996), 40–41.

[15] Mustard, D.
Uncertainty principles invariant under the fractional Fourier transform.
Journal of the Australian Mathematic Society, **33**, Series B (1991), 180–191.

[16] The Fractional Fourier Transform.
http://www.ee.bilkent.edu.tr/∼haldun/wileybook.html.

[17] Bargmann, V.
On a Hilbert space of analytic functions and an associated integral transform, Part I.
Communications of Pure and Applied Mathematics, **14** (1961), 187–214.

Location and Imaging of Moving Targets using Nonuniform Linear Antenna Array SAR

By using a linear antenna array, velocity synthetic aperture radar (VSAR) can detect, focus, and locate slowly moving targets well. However, it may mis-locate fast moving targets in the azimuth (cross-range) direction. In this correspondence, we propose a synthetic aperture radar (SAR) with a nonuniform linear antenna array and give a design of the antenna arrangement. It is shown that our proposed nonuniform linear antenna array SAR (NULA-SAR) can locate both slowly and fast moving targets correctly. An integrated NULA-SAR algorithm for moving target imaging is also presented, and it is verified by some simulations.

I. INTRODUCTION

Synthetic aperture radar (SAR) location and imaging of moving targets has attracted much attention in recent decades. It is known that the difficulty of moving target location and imaging is the estimation of moving target position and velocities.

In the single-channel SAR systems, classical methods for moving target imaging are mostly based on the analysis of the azimuth phase history [1–3]. As pointed out in [2], when the targets move fast such

Manuscript received October 25, 2005; revised August 22 and December 15, 2006; released for publication July 26, 2007.

IEEE Log No. T-AES/43/3/908444.

Refereeing of this contribution was handled by P. Lombardini.

This work was partially supported by the China National Science Foundation (CSNF) under Grant 60502012, partially supported by China Ministry Research Foundation under Grant 51407030203JW0141 and partially supported by the China Aerospace Supporting Foundation under Grant J04-2005047. Xia's work was partially supported by the Air Force Office of Scientific Research (AFOSR) under Grant FA9550-05-1-0161.

that their Doppler centroids exceed the pulse repetition frequency (PRF), the radial velocities and, therefore, the azimuth positions of the targets cannot be uniquely estimated. In higher signal-clutter-ratio (SCR) case, some algorithms not subject to the limitation of the PRF have been proposed in [4], [5], and [6], where the velocity estimations are implemented by tracking the positions of targets in the sequence of multi-look SAR images [4], or by computing the skew of the two-dimensional spectral signature [5], or by analyzing the different phase histories under different platform speeds [6], respectively.

In order to suppress the clutter and better detect and image moving targets, some methods based on multi-receiver SAR system have been presented, e.g., space-time-frequency processing [7], multi-channel SAR [8], uniform linear antenna array SAR (called also velocity SAR or VSAR) [9] etc. As reported in [9], in VSAR system, stationary clutter can be rejected, and slowly moving targets (such as walking people) can be properly detected and imaged via digital Fourier transform (DFT) operation on the multiple complex images formed by a uniform linear antenna array, but fast moving targets (such as moving vehicles) may still be mis-located in the azimuth direction due to the 2π modulo folding of the DFT. To overcome the azimuth location ambiguity, multi-frequency VSAR and dual-speed VSAR have been proposed in [10] and [11], respectively, where a higher complexity of the transmitter and receivers (for multi-frequency VSAR) or a higher maneuverability of the platform (for dual-speed VSAR) is required.

We are also interested here in resolving the azimuth location ambiguity. We equip a conventional SAR with a nonuniform linear antenna array and design-specific arrangement of the elements. This new system is named nonuniform linear antenna array SAR (NULA-SAR). In the NULA-SAR system, a series of complex images are formed by the nonuniform linear antenna array, and two (or multiple) subsets are extracted from the image series. In each subset, the moving targets may be separated from the stationary clutter, and the different information between the two (or multiple) subsets and the Chinese remainder theorem (CRT) [12] are used to resolve the azimuth location ambiguity. Therefore, NULA-SAR has the ability not only to suppress clutter but also to locate both slowly and fast moving targets correctly. In comparison with the multi-frequency VSAR [10] and the dual-speed VSAR [11], NULA-SAR does not require higher complexity of the transmitter and the receivers, or the higher maneuverability of the platform, respectively.

This paper is organized as follows. In Section II we introduce the NULA-VSAR model, formulate the solution of azimuth location ambiguity, and analyze the location accuracy. In Section III an integrated NULA-SAR algorithm for moving target imaging is proposed. In Section IV some simulation results of ground moving targets are given to prove the effectiveness of NULA-SAR algorithm.

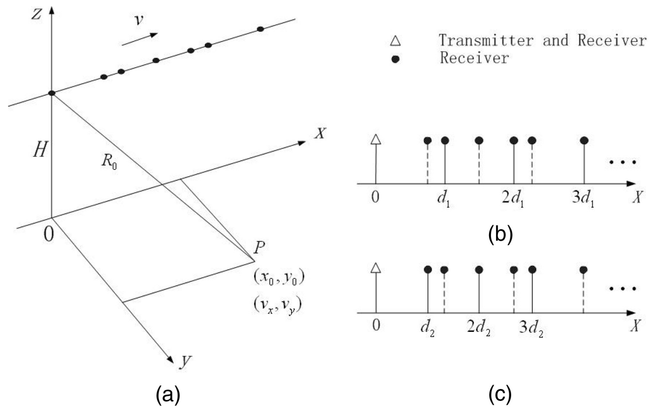

Fig. 1. NULA-SAR geometry.

II. MOVING TARGETS LOCATION USING NULA-SAR

In this section, the NULA-SAR model is introduced first. The azimuth location ambiguity of VSAR is then addressed. The location ambiguity solution using the NULA-SAR is finally presented, and the location accuracy is also studied.

A. NULA-SAR Model

NULA-SAR geometry is illustrated in Fig. 1. X-axis is the azimuth direction and Y-axis is the range direction. The radar platform flies along azimuth direction with altitude H and velocity v. When $t = 0$, a point-like moving target P with constant azimuth-direction speed v_x and range-direction speed v_y is assumed located at $(x_0, y_0, 0)$. At the same time, the transmitter and the first receiver antenna are assumed colocated at $(0,0,H)$, and the other $2M-2$ receiver antennas are arranged at the following coordinates: $(d_1,0,H),(2d_1,0,H),\ldots,((M-1)d_1,0,H)$ and $(d_2,0,H),(2d_2,0,H),\ldots,((M-1)d_2,0,H)$, as shown in Fig. 1(b) and (c), respectively. It is not hard to see that the set Q of all antennas is the union of two subsets Q_1 and Q_2, i.e., $Q = Q_1 \cup Q_2$, where Q_1 and Q_2 are located at instantaneous azimuth coordinate sets $\{vt + md_1; m = 0,1,2,\ldots,M-1\}$ and $\{vt + md_2; m = 0,1,2,\ldots,M-1\}$, respectively. In addition, d_1 and d_2 are two distinct positive real numbers and not integer multiple of each other.

B. Azimuth Location Ambiguity of VSAR

Note that Q_1 is a uniform array composed of M elements with spacing d_1. Firstly, let us review the VSAR location processing in Q_1.

After the range compression and the azimuth focusing, the image of P formed by the mth antenna of Q_1 may be represented as [9, 10]

$$S_{1,m}(n,l) = \exp\left(-j2\pi\frac{\rho_x n_0 m d_1}{R_0\lambda}\right) \cdot \delta(n - n_0 - \Delta_{\text{shift}}) \cdot \delta(l - l_0) \tag{1}$$

where the amplitude and the constant phase term is ignored for convenience; R_0 is the distance from the transmitter to P at $t = 0$, i.e., $R_0 = \sqrt{x_0^2 + y_0^2 + H^2}$; λ is the carrier wavelength; l_0 is certain range cell where P locates after the range compression; n_0 and Δ_{shift} are quantization results of x_0 and target's azimuth migration by the azimuth resolution ρ_x, respectively. As pointed out in [9], [10], Δ_{shift} may be represented as

$$\Delta_{\text{shift}} = (x_0 v_x + y_0 v_y)/(v\rho_x). \tag{2}$$

The problem of interest herein is to locate P at its true azimuth position n_0. To do so, Δ_{shift} must be estimated accurately and subtracted from the detected position $(n_0 + \Delta_{\text{shift}})$. Multiplying the phase factor $\exp[j2\pi(n_0 + \Delta_{\text{shift}})\rho_x md/(R_0\lambda)]$ to with the knowledge of the detected position $(n_0 + \Delta_{\text{shift}})$, (1) becomes

$$S_1(m) = \exp\left(j2\pi\frac{\rho_x \Delta_{\text{shift}} m d_1}{R_0\lambda}\right) \cdot \delta(n - n_0 - \Delta_{\text{shift}}) \tag{3}$$

for $m = 0, 1, \ldots, M - 1$. Defining the normalized frequency

$$f_1 = \rho_x \Delta_{\text{shift}} d_1/(R_0\lambda) \tag{4}$$

(3) can be rewritten as

$$S_1(m) = \exp(j2\pi f_1 m) \cdot \delta(n - n_0 - \Delta_{\text{shift}}) \tag{5}$$

which shows clearly that f_1 and, therefore, Δ_{shift} can be estimated via DFT of $S_1(m)$ in terms of m. In the M-point DFT results (defined as V-images in [9] and detailed definition is given in the Appendix), we have $f_1' = \text{mod}(f_1, 1)$ that is the residue of f_1 due to the 2π folding operation of the DFT. If P moves slowly such that $0 \le f_1' = f_1 < 1$, f_1 and, therefore, Δ_{shift} can be estimated in the V-images, and thus there is no location ambiguity in this case. Otherwise, if P moves fast such that $f_1 = f_1' + K_1$ for an unknown integer K_1, the estimation of Δ_{shift} will not be determined uniquely by using a single residue f_1' i.e., the location ambiguity will occur. This is the reason why in a VSAR system walking people can be located, but moving vehicles may not be positioned correctly [9]. To overcome the location ambiguity, a multi-frequency VSAR system has been proposed in [10], where multiple carrier wavelengths λ are used such that multiple DFTs can be applied to these data from multiple carrier wavelengths, and multiple residues of f_1 can be obtained in (4), and then Δ_{shift} can be determined uniquely by CRT. The dual-speed VSAR [11] is also based on the similar idea. From (4) we note that multiple antenna-spacings d_1 also can produce multiple residues of f_1. This is the idea of the following NULA-SAR accurate location for moving targets by using multiple groups of antennas with distinct spacings.

C. NULA-SAR Location Principle

Now we perform DFT not only along antennas in Q_1 but also along antennas in Q_2. Like the above analysis, from (4) and (5), we directly have

$$f_2 = \rho_x \Delta_{\text{shift}} d_2/(R_0\lambda) = f_2' + K_2 \tag{6}$$

$$S_2(m) = \exp(j2\pi f_2 m) \cdot \delta(n - n_0 - \Delta_{\text{shift}}). \tag{7}$$

where $S_2(m)$ is the focused image of P obtained at the mth antenna of Q_2, $f_2' = \text{mod}(f_2, 1)$, K_2 is an unknown integer. Let $L_i = R_0\lambda/(\rho_x d_i)$, (4) and (6) show

$$\Delta_{\text{shift}} = (f_i' + K_i)L_i \tag{8}$$

which means

$$f_i' L_i = \text{mod}(\Delta_{\text{shift}}, L_i) \tag{9}$$

for $i = 1, 2$. Therefore, the moving target location problem is equivalent to determine the value of Δ_{shift} from its two residues $f_i' L_i$, for $i = 1, 2$. By using the CRT, Δ_{shift} can be uniquely determined if it is less than the least common multiple of L_1 and L_2 (expressed $\text{LCM}(L_1, L_2)$ for short). Once Δ_{shift} is known, the moving target P can be located correctly by subtracted Δ_{shift} from the detected position $(n_0 + \Delta_{\text{shift}})$, i.e., the azimuth location ambiguity can be resolved.

If only one subset Q_1 or Q_2 is employed, $\text{LCM}(L_1, L_2)$ is reduced to L_1 or L_2 accordingly. Because d_1 and d_2 are assumed not integer multiples of each other, L_1 and L_2 are not integer multiples of each other accordingly. Hence $\text{LCM}(L_1, L_2) > L_i$ for $i = 1, 2$. Therefore, the maximal determinable value of Δ_{shift} can be increased over the one when only one subset Q_i is employed, which corresponds to that the maximal determinable velocity (or blind speed in radar jargon) of the moving target can be increased (see (2)). In (2), the term $x_0 v_x$ can generally be neglected, because $y_0 \approx R_0$ and x_0 is usually much smaller than y_0. Thus the determinable upper limit of Δ_{shift} can be represented as

$$\Delta_{\text{shift,max}} \approx R_0 v_{y,\text{max}}/(v\rho_x) = \text{LCM}(L_1, L_2) \tag{10}$$

and then the blind (maximal) speed of NULA-SAR is

$$|v_{y,\text{max}}| = \frac{1}{2} \cdot \frac{v\rho_x \text{LCM}(L_1, L_2)}{R_0} \tag{11}$$

where 1/2 is multiplied because there are two different possible directions of v_y, toward and away from the radar, respectively.

In practice, the size of an antenna array is limited by the allowed space in a radar platform, and the number of antennas is limited by allowed complexity of the system. Hence, it is worth comparing the location performances between NULA-SAR and uniform linear antenna array SAR, i.e., VSAR, with the same size of antenna array and the same number of antennas. Without loss of generality, we assume $d_2 < d_1$. According to the model of NULA-SAR, the array size is $Z = (M-1)d_1$, that is assumed predefined array size of the radar platform. The antenna number of NULA-SAR $N \le 2M-1$, where the equality holds if and only if $Q_1 \cap Q_2 = \Phi$ (Φ means the empty set). If a VSAR with N elements is set in Z, its inter-element spacing is

$$d_0 = \frac{Z}{N-1} \ge \frac{(M-1)d_1}{2M-2} = d_1/2. \tag{12}$$

From (4), (12), and the definition of L_1, one can see that the maximal determinable value of Δ_{shift} using this VSAR is $2L_1$. As mentioned above, $\text{LCM}(L_1,L_2) > L_1$, i.e., $\text{LCM}(L_1,L_2) \ge 2L_1$. Thus for the same array size and the same number of antennas, NULA-SAR can get larger determinable range of Δ_{shift} than VSAR. In other words, the blind speed of NULA-SAR is above the one of VSAR without increasing the antenna spacing and the complexity of the system.

D. Study on Location Accuracy

What was studied above provides the basic idea of Δ_{shift} estimation by using the CRT in the V-images, which is based on two assumptions: 1) L_i are integers; 2) the estimated residues f_i' in the V-images are accurate, for $i = 1,2$. However, in practice these assumptions may not hold. In particular, small estimation error of f_i' will cause large estimation error of Δ_{shift}. Now we analyze the effect of the estimation error of f_i' on the location accuracy.

The zero-padded N_{DFT}-point DFT on (5) and (7) in terms of m gives

$$f_i' = \frac{N_i}{N_{\text{DFT}}} + \varepsilon_i \tag{13}$$

where N_i are certain integers with $0 \le N_i < N_{\text{DFT}}$ and they are directly obtained in the DFT results, ε_i are the uncertain errors, and $\varepsilon_i \le 1/(2N_{\text{DFT}})$, for $i = 1,2$. Accordingly, (8) can be rewritten as

$$\Delta_{\text{shift}} = \frac{N_i}{N_{\text{DFT}}} L_i + K_i L_i + \varepsilon_i L_i \tag{14}$$

where L_i does not need to be integers, for $i = 1,2$. When $N_{\text{DFT}} > L_1 + L_2$, the robust CRT [10] gives

$$\hat{\Delta}_{\text{shift}} = \frac{R_0\lambda}{2\rho_x} \sum_{i=1}^{2} \left(K_i + \frac{N_i}{N_{\text{DFT}}} \right) \cdot \frac{1}{d_i} \tag{15}$$

where K_i are determined by

$$(K_1,K_2) = \underset{\substack{0 \le \bar{K}_1 < \text{LCM}(L_1,L_2)/L_1 \\ 0 \le \bar{K}_2 < \text{LCM}(L_1,L_2)/L_2}}{\arg\min} \left| \bar{K}_1 L_1 + \frac{N_1}{N_{\text{DFT}}} L_1 - \bar{K}_2 L_2 - \frac{N_2}{N_{\text{DFT}}} L_2 \right|$$
$$\text{for integer pair } (\bar{K}_1,\bar{K}_2). \tag{16}$$

The accuracy of the solution of Δ_{shift} in (15) can be estimated as

$$|\Delta_{\text{shift}} - \hat{\Delta}_{\text{shift}}| \le \frac{R_0\lambda}{4N_{\text{DFT}}\rho_x} \sum_{i=1}^{2} \frac{1}{d_i}. \tag{17}$$

This means that the location error can be reduced by increasing N_{DFT}. If the location error is limited within an azimuth cell, i.e., let $|\Delta_{\text{shift},i} - \hat{\Delta}_{\text{shift},i}| < 1$, the N_{DFT} needs to satisfy

$$N_{\text{DFT}} > \frac{R_0\lambda}{4\rho_x} \sum_{i=1}^{2} \frac{1}{d_i}. \tag{18}$$

About the details of the robust CRT, we refer the reader to [10].

III. NULA-SAR ALGORITHM FOR MOVING TARGET IMAGING

Based on the moving target accurate location studied above, a NULA-SAR algorithm for moving target imaging is presented below. All the following steps, except Step 7, are common operations for Q_1 and Q_2.

Step 1 Two-dimensional matching filter with the impulse response function of the stationary scene is used to obtain the scene image.

Step 2 Perform M-point DFT along the antenna array direction to get the V-images.

Step 3 Remove the 0th V-image, i.e., replace the 0th V-image by 0, to reject the clutter. The detailed discussion about this step is in the Appendix.

Step 4 Perform M-point inverse DFT along the antenna array direction.

Step 5 In the range cell where a moving target is detected, estimate the chirp rate of the azimuth signal by applying the method proposed in [13], and then focus the target by compensating the corresponding quadratic phase term.

Step 6 Carry out zero-padded N_{DFT}-point DFT along the antenna array direction to get the new V-images.

Step 7 In new V-images, estimate Δ_{shift} according to (15), as described in previous section.

Step 8 Take N_{DFT}-point inverse DFT along the antenna array direction.

Step 9 Relocate the moving target in terms of the estimated Δ_{shift}.

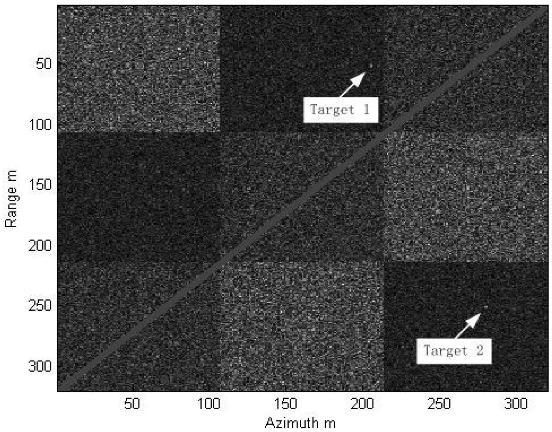

Fig. 2. VSAR image before moving target location.

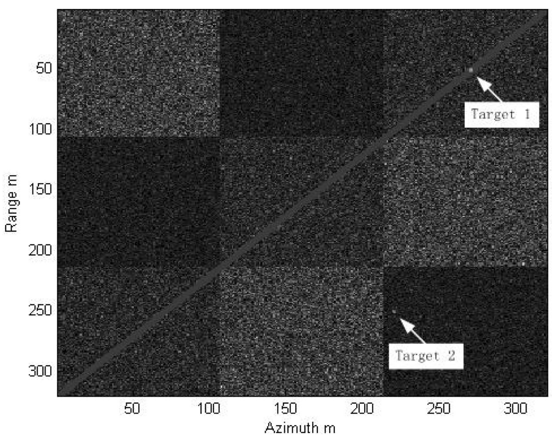

Fig. 3. VSAR image of Q_1 after locating moving targets on scene.

IV. SIMULATION RESULTS

To verify the above NULA-SAR algorithm, some simulations are presented in this section. The parameters are: platform speed $v = 200$ m/s, altitude $H = 4000$ m, wavelength $\lambda = 0.03$ m, PRF = 1 kHz, $\rho_x \approx 1$ m, $R_0 \approx 10$ km, the number of antennas $M = 8$, and the inter-element spacings of Q_1 and Q_2 are $d_1 = 2.0$ m and $d_2 = 1.5$ m, respectively.

In the simulation, the static scene is composed of several fields with different reflectivities and a road with 45° azimuth angle. There are two moving targets in the scene, the first one of which moves away from the radar with speed 1.84 m/s, while the second one moves toward the radar with speed 5.94 m/s. Their corresponding range-direction velocities are -1.30 m/s and 4.20 m/s. For each target, SCR is assumed to be equal to 5 dB. From (11), we can calculate that the blind speed of the NULA-SAR is 6 m/s, while the blind speeds are 1.5 m/s and 2 m/s, respectively, when Q_1 or Q_2 is used alone. Before moving target location, the VSAR image obtained by Q_1 or Q_2 is shown in Fig. 2, where the targets shift out of the road due to their shifted Doppler centroids. After locating the moving targets on the scene, the VSAR imaging results formed by Q_1 and Q_2 are shown in Fig. 3 and Fig. 4, respectively, where the first target is located correctly while the second one is also mis-located by both Q_1 and Q_2. This is because that the range-direction speed of the first target is below the blind speeds of Q_1 and Q_2, while the one of the second target is above the blind speeds of Q_1 and Q_2. Fig. 5(a) and (b) show the V-images formed by Q_1 and Q_2, respectively, where N_{DFT} is set to 512 to satisfy (18) and $N_{\mathrm{DFT}} > L_1 + L_2$. Using the difference between Fig. 5(a) and (b), we can estimate the azimuth locations of the targets accurately with (15). The NULA-SAR imaging result after locating the moving targets on the scene is shown in Fig. 6, where the targets are located correctly on the road.

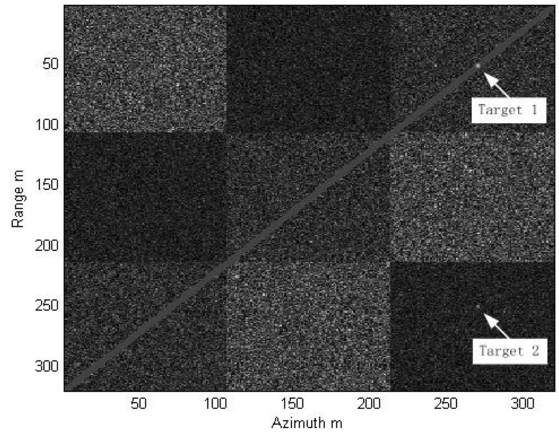

Fig. 4. VSAR image of Q_2 after locating moving targets on scene.

V. CONCLUSION

A NULA-SAR system is proposed in this paper. It is shown that, by dividing a nonuniform linear antenna array into two subsets and using multiple complex images from these two subsets, NULA-SAR cannot only suppress the clutter but also locate both slowly and fast moving targets correctly. An integrated NULA-SAR algorithm for moving target imaging is also proposed. Simulation results show the effectiveness of the NULA-SAR algorithm. As a remark, although only two subsets of the antennas are employed in this correspondence, it can be straightforwardly generalized to a general number of subsets with different spacings d_i in the ith subset.

APPENDIX (DISCUSSION ABOUT CLUTTER SUPPRESSION)

Before estimating Δ_{shift}, the clutter must be suppressed, otherwise the detected position $(n_0 + \Delta_{\mathrm{shift}})$ is difficult to be found, especially when the SCR is not too high. Like the analysis in [10], we also choose interval $[0, 1)$ as the normalized main period of DFT. Therefore, in the results of the M-point

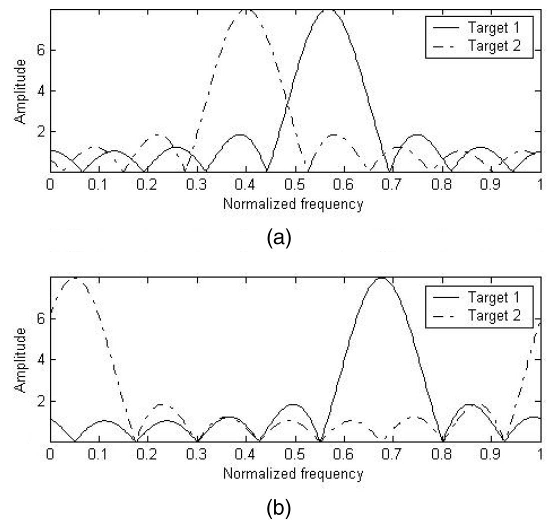

Fig. 5. V-images of moving targets. (a) V-images at Q_1. (b) V-images at Q_2.

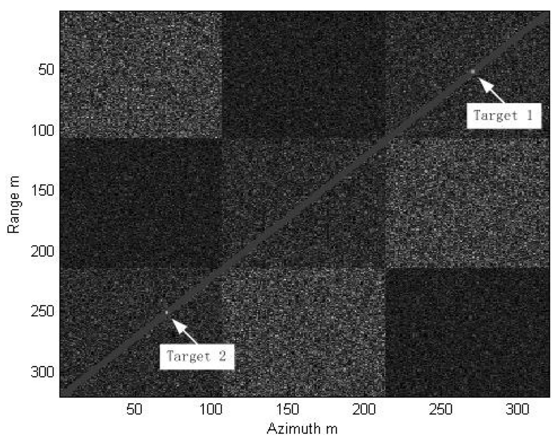

Fig. 6. NULA-SAR image after locating moving targets on scene.

DFT along Q_1 or Q_2 at every pixel of the M SAR images, the ith channel corresponds to the normalized frequency i/M, for $i = 0, 1, \ldots, M-1$. All of the ith channels at all pixels after the M-point DFT compose the ith V-image. From (2), (4), and (6), one can see that, in the results of the DFT along Q_1 or Q_2, $f_1 = f_2 = 0$ for stationary targets, i.e., the stationary targets stand in the 0th V-image formed at Q_1 or Q_2. Thus the stationary clutter can be suppressed by removing the 0th V-image, i.e., replacing the 0th V-image by 0. Occasionally, the moving target may also stand in the 0th V-image due to the 2π folding operation of DFT, and it may be removed in company with the clutter. But it is impossible that the moving target stands in both 0th V-images formed at Q_1 and Q_2. (Proof: if the moving target stands in both 0th V-images formed by Q_1 and Q_2, we have $\Delta_{\text{shift}} = K_1 L_1 = K_2 L_2$. This means $\Delta_{\text{shift}} = K \cdot \mathrm{LCM}(L_1, L_2)$ for a certain integer K. Because of the restriction of $\Delta_{\text{shift}} < \mathrm{LCM}(L_1, L_2)$, we have $K = 0$ and $\Delta_{\text{shift}} = 0$. Moreover, $x_0 \ll y_0$ and the values of v_x and v_y are comparable, thus $\Delta_{\text{shift}} = 0$ is hold if and only if $v_x = v_y = 0$ (see (2)). This is inconsistent with the fact that the target is moving.) Therefore, Δ_{shift} also can be determined by the CRT, where one of its two residues is equal to zero. This discussion about the clutter suppression is similar to the one in multi-frequency VSAR [10]. Also, it is necessary to explain the difference of the DFT between Step 2 and Step 6. In Step 2, M-point DFT is enough to separate the moving targets from the clutter, because the frequency resolution of the DFT is $1/M$ that is limited by the Rayleigh bound. In Step 6, the purpose of using zero-padded N_{DFT}-point DFT is to improve the frequency estimation accuracy.

GANG LI
JIA XU[1]
YING-NING PENG
Dept. of Electronic Engineering
Tsinghua University
Bejing 100084
China

XIANG-GEN XIA
Dept. of Electrical and Computer Engineering
University of Delaware
Newark, DE 19716
E-mail: (xxia@ee.udel.edu)

[1]Also with Radar Academy of Airforce Wuhan, 430010 China.

REFERENCES

[1] Werness, S. A. S., Carrara, W. G., Joyce, L. S., and Franczak, D. B.
Moving target imaging algorithm for SAR data.
IEEE Transactions on Aerospace and Electronic Systems, **26**, 1 (1990), 57–67.

[2] Barbarossa, S.
Detection and imaging of moving objects with synthetic aperture radar.
IEE Proceedings, Pt. F, **139**, 1 (1992), 79–88.

[3] Perry, R. P., DiPietro, R. C., and Fante, R. L.
SAR imaging of moving targets.
IEEE Transactions on Aerospace and Electronic Systems, **35**, 1 (1999), 188–200.

[4] Kirscht, M.
Detection and imaging of arbitrarily moving targets with single-channel SAR.
IEE Proceedings—Radar Sonar & Navigation, **150**, 1 (2003), 7–11, 2003.

[5] Marques, P., and Dias, J.
Velocity estimation of fast moving targets using a single SAR sensor.
IEEE Transactions on Aerospace and Electronic Systems, **41**, 1 (2005), 75–89.

[6] Wang, G., Xia, X.-G., and Chen, V. C.
Dual-speed SAR imaging of moving targets.
IEEE Transactions on Aerospace and Electronic Systems, **42**, 1 (2006), 368–379.

[7] Barbarossa, S., and Farina, A.
Space-time-frequency processing of synthetic aperture radar signals.
IEEE Transactions on Aerospace and Electronic Systems, **30**, 2 (1994), 341–358.

[8] Ender, J.
Detection and estimation of moving target signals by multi-channel SAR.
In *Proceedings of EUSAR'96 Conference*, 1996, 411–417.

[9] Friedlander, B., and Porat, B.
VSAR: A high resolution radar system for detection of moving targets.
IEE Proceedings—Radar, Sonar & Navigation, **144**, 4 (1997), 205–218.

[10] Wang, G., Xia, X.-G., Chen, V. C., and Fiedler, R. L.
Detection, location, and imaging of fast moving targets using multifrequency antenna array SAR.
IEEE Transactions on Aerospace and Electronic Systems, **40**, 1 (2004), 345–355.

[11] Li, G., Xu, J., Peng, Y.-N., and Xia, X.-G.
Moving target location and imaging using dual-speed velocity SAR.
IET Radar Sonar & Navigation, **1**, 2 (2007), 158–163.

[12] McClellan, J. H., and Rader, C. M.
Number Theory in Digital Signal Processing.
Englewood Cliffs, NJ: Prentice-Hall, 1979.

[13] Wood, J., and Barry, D.
Linear signal synthesis using the Radon-Wigner transform.
IEEE Transaction on Signal Processing, **42**, 8 (1994), 2105–2111.

Weather Radar Equation Correction for Frequency Agile and Phased Array Radars

This paper presents the derivation of a correction to the Probert-Jones weather radar equation for use with advanced frequency agile, phased array radars. It is shown that two additional terms are required to account for frequency hopping and electronic beam pointing. The corrected weather radar equation provides a basis for accurate and efficient computation of a reflectivity estimate from the weather signal data samples. Lastly, an understanding of calibration requirements for these advanced weather radars is shown to follow naturally from the theoretical framework.

I. INTRODUCTION

The classical weather radar equation was introduced by Probert-Jones in 1962 [1] and has since been universally used to implement reflectivity algorithms. These algorithms are used to compute reflectivity estimates from the signal sample data collected by weather radars. Existing weather radars typically operate at a fixed frequency and employ antennas that are mechanically scanned. Recently however, there has been interest in adding a weather processing capability to advanced radars originally developed for other purposes. Some of these radars are frequency agile and use phased array antennas. Adaptive waveforms and phased array technology for agile beam scanning strategies have also been identified as technologies that should be investigated for the next generation of U.S. national weather radars [2].

The cross section density of precipitation in the Rayleigh region varies with frequency, as does antenna gain and beamwidth. Further, antenna gain and beam solid angle also vary when the beam of a planar phased array is electronically pointed off broadside. These inter-related effects impact the radar effective radiated power, the size of the radar resolution cell and ultimately the observed average power return and reflectivity estimate. These effects raise doubts about the direct applicability of the Probert-Jones equation to these radars. If used, the classical Probert-Jones weather radar equation would lead to reflectivity errors because frequency hopping and electronic beam pointing effects are not inculded. These errors would exceed the reflectivity accuracy objectives of most modern weather radars. The objective of the work described here is to analytically account for the effects of weather radar frequency agility and electronic beam pointing in the weather radar equation. Analytically accounting for these effects leads to a theoretical result that permits a reflectivity estimate to be computed simply, accurately, and efficiently. The theoretical framework also leads to a clear understanding of the calibration requirements for frequency agile, phased array weather radars.

Manuscript received May 1, 2006; revised November 24, 2006 and July 18, 2007; released for publication July 18, 2007.

IEEE Log No. T-AES/43/3/908445.

Refereeing of this contribution was handled by E. S. Chornoboy.

This work was supported in part by the Office of Naval Research through a Cooperative Research and Development Agreement, NCRADA-NPS-03-0052, between Naval Postgraduate School, Monterey, CA and ProSensing, Inc., Amherst, MA.

II. PHASED ARRAY FUNDAMENTALS

A. Scanned Array Gain

Consider a rectangular planar array with separable aperture distribution

$$E_a(x,y) = E_{a1}(x)E_{a2}(y) \tag{1}$$

where $E_{a1}(x)$ and $E_{a2}(y)$ are the aperture field distributions in the x and y directions, respectively. It can be shown [3] that when the aperture distribution is separable, the directivity D is also separable and is given by

$$D = \pi D_x D_y \cos\theta \tag{2}$$